Separation and Purification Technology 352 (2025) 128046

Contents lists available at ScienceDirect

Separation and Purification Technology

journal homepage: www.elsevier.com/locate/seppur

Modelling a countercurrent liquid centrifuge for large-scale isotope separation

Joseph F. Wild *, Zhinan Han, Yuan Yang *

Department of Applied Physics and Applied Mathematics, Columbia University, New York, NY 10027, United States

ARTICLE INFO

Editor: Raquel Aires Barros

Keywords:
Isotope separation
Centrifuge
Chemical engineering
Nuclear energy
Nuclear medicine
Countercurrent centrifuge

ABSTRACT

Advances across various fields of science and medicine have been significantly influenced by enriched natural isotopes since the dawn of the nuclear age. Unfortunately, many elements cannot be processed using common high-throughput techniques such as gas centrifugation or gas distillation due to their inability to form stable gases near room temperature. This paper evaluates the use of liquid phase centrifugation as a versatile method for the high-throughput separation of these elements. By modeling a countercurrent liquid centrifuge and analyzing its integration into a cascading system, we demonstrate its potential efficiency and versatility. The findings suggest that liquid centrifugation can achieve attractive throughput rates for a wide range of elements, providing a general solution for isotope separation. Potential challenges and limitations are also discussed.

1. Introduction

Enriched isotopes remain essential for uncovering scientific mechanisms and developing new technologies and methods. In particular, the large-scale separation of certain isotopes such as ^{235}U, ^{2}H, ^{13}C, ^{15}N, ^{18}O, and ^{100}Mo have greatly accelerated science, technology, and medicine [1–5]. However, these high-throughput, low-cost separation technologies are incompatible with most elements, as they require gaseous species to operate, such as in gas centrifugation, distillation, and diffusion [6]. For the majority of elements on the periodic table there is no stable or safe gaseous molecule which exists near ambient temperatures and pressures. Instead, electromagnetic isotope separation (EMIS) is dominant in these cases but can only produce isotopes at the 1 mg–1 kg scale annually for these elements [6,7]. These limitations hinder science and medicine in known and unknown ways, for example, ^{48}Ca (naturally 0.19 %) in our inability to accurately test the existence of neutrinoless double beta decay [8], ^{46}Ti (8.25 %) and ^{54}Fe (5.85 %) for developing the strongest and lightest alloys possible [9,10], ^{6}Li/^{7}Li (7.5/92.5 %) for nuclear energy applications, and numerous precursors for medical radioisotopes which may find unknown uses if they could be produced in large enough quantities to be thoroughly tested [11,12].

Here, we model and analyze the recently reported liquid phase centrifugation method as a potential technology for separating most natural isotopes on a kg-ton/year scale [13]. The primary goal of this study is to explore the technology using first-principle flux equations. This approach is attractive because it addresses the significant limitations of traditional gas centrifuges, which are restricted to elements that can form stable gaseous phases. In general, it is found that there are substantial similarities between theoretical liquid centrifuges and existing gas centrifuges of the same size and rotational speeds. Both centrifugation methods share process engineering and cascading considerations, while the production rate of material reduces to a function of properties of the working fluid, such as the diffusion coefficient, partial density, and temperature.

2. Equations and model

2.1. Governing equations

According to the derivations in Section S1 of the supporting information, the transport of ions, atoms, and molecules within a spinning centrifuge is governed by Eq. (1) and Eq. (2).

$$\vec{J}_i = u_i\left[-RT\nabla c_i - RT\nabla c_s\frac{\partial ln(\gamma_s)}{\partial ln(X_s)}\frac{c_i}{c_s} + \omega^2\vec{r}c_iM_i(1 - \bar{v}_i\rho_{soln}) + c_iz_iF\vec{E}\right] + c_i\vec{V} \quad (1)$$

$$with\ \frac{\partial c_i}{\partial t} = -\nabla\bullet\left(\vec{J}_i\right) \quad (2)$$

* Corresponding authors.
E-mail addresses: jfw2127@columbia.edu (J.F. Wild), yy2664@columbia.edu (Y. Yang).

https://doi.org/10.1016/j.seppur.2024.128046
Received 2 April 2024; Received in revised form 15 May 2024; Accepted 20 May 2024
Available online 22 May 2024

Nomenclature

α	Isotope separation factor, Dimensionless
γ	Activity coefficient, Dimensionless
ρ	Density, kg/m^3
ω	Angular velocity, rad/s (RPM)
c	Molar concentration, mol/m^3
D	Diffusion coefficient, m^2/s
E	Electric field strength, V/m
F	Feed flowrate, kg/s (g/hr)
F	Faraday constant, 96,485 C/mol
h	Centrifuge height, m
J	Molar flux, mol/m^2/s
L	Countercurrent flowrate, kg/s (g/hr)
M	Molecular mass, kg/mol
n	Neutron difference, Dimensionless
N	Isotope ratio, Dimensionless
P	Product flowrate, kg/s (g/hr)
P	Pressure, Pa
r	Radius, m
R	Gas constant, 8.314 J/mol/K
SWU	Separative Work Units, Dimensionless
t	Time, s
T	Temperature, K
u	Mobility, mol·s/kg
δU	Separative power, s^{-1} (yr^{-1})
$\bar{v}$	Partial specific volume, m^3/kg
V	Velocity, m/s
W	Waste flowrate, kg/s (g/hr)
X	Mole fraction, Dimensionless
z	Species charge, Dimensionless

Where $\vec{J}_i$ is the molar flux of species *i*. The subscript *i* is for a certain isotopic species, while *s* includes all isotopes with the same atomic number as species *i*. *u* is the mobility, *R* and *T* are the molar gas constant and temperature, respectively, *c* is the molar concentration, γ is the activity coefficient, and *X* is the mole fraction. ω is the rotational velocity, $\vec{r}$ is the radial vector from the rotation axis, *M* is the molar mass, $\bar{v}$ is the partial specific volume, and ρ_{soln} is the solution density at $\vec{r}$. *z* is the species charge, ***F*** is the Faraday constant, and $\vec{E}$ is the electric field. $\vec{V}$ is the velocity field of the fluid and *t* is time.

Many of the components of Eq. (1) are functionally identical to the counterpart gas centrifuge equations, specifically the diffusion, centrifugal, and advection terms (terms 1, 3 and 5 on the right, respectively) [14]. $\vec{V}$ is for the whole fluid, and applies to the solvent and all solutes. The primary difference for the liquid solution case is the non-ideal and electrostatic terms (2 and 4, respectively) to account for the interaction of the solvent and ions. In considering isotope transport in a pure neutral liquid (e.g., ^{1}H/^{2}H and ^{16}O/^{18}O in H_2O, and ^{35}Cl/^{37}Cl and ^{46}Ti/^{48}Ti in $TiCl_4$), term 4 is zero as $z_i = 0$ and term 2 is 0 since isotope mixing is ideal. Therefore, in a pure neutral liquid, Eq. (1) can be simplified to Eq. (3) where D_i is the self-diffusion coefficient of the liquid.

$$\vec{J}_i = -D_i\nabla c_i + D_i\frac{\omega^2\vec{r}}{RT}c_iM_i(1-\bar{v}_i\rho_{soln}) + c_i\vec{V} \tag{3}$$

The advection term in Eq. (1) and (3) now requires Navier-Stokes Equations (NSE) for incompressible fluids, rendering Eq. (1) and (3) analytically intractable, even in the steady-state when the left side of Eq. (2) is zero. The equations therefore require discretization and computational solutions. Incompressibility is assumed since the bulk modulus of liquids is typically 1–3 GPa, whereas the pressure inside a liquid centrifuge will have a maximum around 100–150 MPa at the outer radii [15].

The discretization of the cylindrical centrifuge was achieved in two dimensions, *r* and *z*, representing the radius and height, respectively. The azimuthal angle is neglected due to the rotational symmetry of the centrifuge. A staggered grid finite difference method with first order central difference was used to discretize and solve Eqs. (1), 2, and 3. An overview schematic is shown in Fig. 1 and further details of the discretization is given in Section S2 of the supporting information.

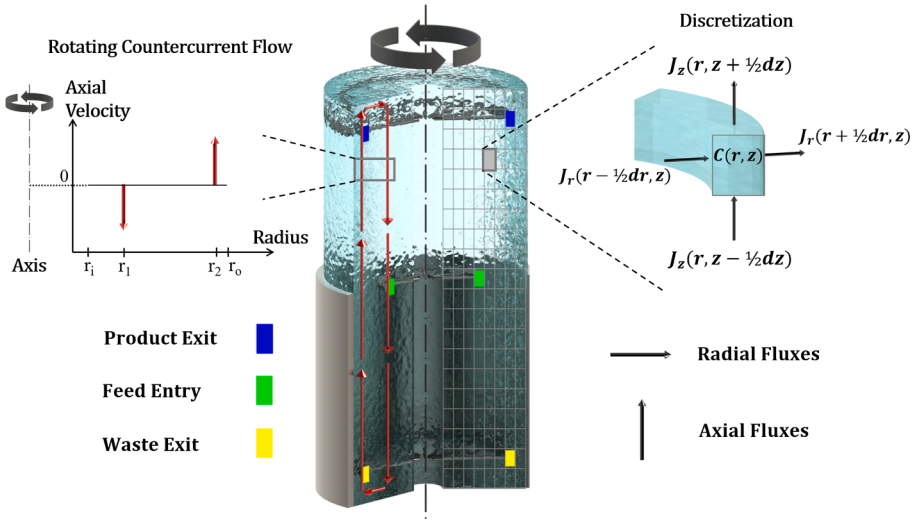

Fig. 1. A cross-section schematic of a discretized countercurrent liquid centrifuge. The rotating countercurrent flow profile is shown by the red circulating arrows. The feed, product, and waste streams flow into and out of the centrifuge through channels connected to the central axis. The change in isotope concentration for each finite element volume is determined by the incoming and outgoing fluxes with time. The flow profile between the inlet and outlets is found by solving the Navier Stokes Equations. Centrifugal forces generate modest radial isotope gradients, then countercurrent flow multiplies this into large axial isotope gradients. (For interpretation of the references to colour in this figure legend, the reader is referred to the web version of this article.)

2.2. Fluid velocity field and countercurrent flow

The advection term, $c_i\vec{\boldsymbol{V}}$, requires greater attention since the velocity profile is not defined in terms of prior-known parameters of the centrifuge or fluid. Instead, the velocity profile arises from hydrodynamic equations of fluid flow, which are in turn informed by the introduction of the countercurrent flow and how the fluid is flowed into and out of the centrifuge. It is the introduction of the countercurrent flow profile which can significantly enhance the separation efficiency of a centrifuge, whereas the feed flow continuously introduces and extracts material from the constantly rotating system. Each flow pattern, quantified by its overall magnitude – $L[kgs^{-1}]$ for the countercurrent flow and $F[kgs^{-1}]$ for the feed flow – significantly influences the centrifuge's behavior, representing key parameters for optimization.

We simulate countercurrent flow using a two-shell profile (Fig. 1), with further details available in *Cohen (1951)* [14]. Here, one stream of fluid is moving axially upwards at a radius r_2, very close to the outer radius r_o, while a second stream, which is equal in mass flow magnitude, travels downwards at some intermediate radius $r_i < r_1 < r_2$. These flows are connected to one another at the top and bottom of the centrifuge to form a closed loop of constant flow. The magnitude of the countercurrent flow, L, is defined by the mass flow rate travelling along one of the streams. In all simulations, the inner stream was within two radial finite element volumes, while the outer stream was at the outer two radial finite element volumes.

Centrifugal forces alone generate modest radial isotope gradients and separation factors, as given by the elementary separation factor, α_o, in Eq. (4) for a 1D centrifuge in r, radius [13]. Countercurrent flow then effectively multiplies α_o into large axial isotope gradients along the length of the centrifuge between the two outlet locations, resulting in the overall separation factor, α, given in Eq. (5) for two isotopic species M_1 and M_2.

$$\alpha_o = exp\left(\frac{\omega^2(M_2 - M_1)\left(r_o^2 - r_i^2\right)}{2RT}\right) \tag{4}$$

$$\alpha = \frac{\left([M_2]/[M_1]\right)_{outlet1}}{\left([M_2]/[M_1]\right)_{outlet2}} \tag{5}$$

The feed flow, F, represents the magnitude of material which is constantly flowing through the centrifuge from its single inlet to its two outlets. These outlets are where the enriched and depleted products are collected. Since liquids are essentially incompressible, the introduction and removal of the fluid will drive a velocity profile within the centrifuge which satisfies the continuity and momentum equations of the Navier-Stokes Equations (NSE) for incompressible flow. The velocity profile from the feed flow is calculated by solving the NSE using the SIMPLE algorithm over a 2D domain in r and z with the inlet, outlets, fluid properties, and boundaries defined [16]. This was also achieved in MATLAB and was computed at the beginning of each simulation in a separate function using the parameters defined.

In application centrifuges, the way in which the countercurrent and feed flows are induced and controlled depends on the overall design, which is a decision made by centrifuge engineers and is not discussed here [17]. In the case of the model, each flow contributes to the advection term, $\vec{\boldsymbol{V}}$, and their contribution to the overall separation is the focus of this work. Generally, the notable similarities between the governing equations for liquids and gases could yield predictable results, indicating comparable behaviors for these two systems. However, despite the similarities, there still several fundamental differences which are likely to be impactful, particularly in application centrifuges: 1) Fluid properties, including ρ, D, and viscosity ν. 2) Inducing the countercurrent. 3) Extracting the streams. 4) Wall stresses, which will be discussed in the following sections.

3. Results

3.1. Computational results

Before discussing the results, it is worth pointing out that published analytical solutions exist for the steady-state gas case [18,19]. These are discussed in more detail in Section S3 and Fig. S2 of the S.I., which details how the fluid and centrifuge parameters effect the separation factor and separative power. This means that these can be used as both a comparison and a validation for some of the expected trends of the state-state behavior.

Firstly, there are two broad cases to analyze: 1) Pure liquids and 2) dissolved salts. The pure liquid case will be assessed here since the results are easier to generalize across elements and molecules, while the counterpart plots are presented in Fig. S3 of the S.I. for a selected salt ($CaCl_2$), and the generalization of this is discussed. α is defined as the separation factor between the two outlet locations. In all cases, $ln(\alpha)$ is expressed for an isotope mass difference of $\Delta M = 0.001\ kgmol^{-1}$, which is the case for isotopes differing by one neutron. This separation factor does not depend on the initial ratio of the isotopes.

A centrifuge of height $h = 100$ cm, $r_i = 2.5$ cm, $r_o = 7.5$ cm, and peripheral velocity $v_o = \omega r_o = 471$ ms^{-1} ($\omega = 60$ kRPM) is used for all simulations where these parameters are not themselves varied. These parameters are chosen since they are the same as typical early gas centrifuges used for testing which allows for comparisons (e.g. G-2 in German pilot plant SP2) [20]; however, the dimensions of prototype and application liquid centrifuges could vary considerably depending on the rotor material and fluid used. The centrifuge is discretized into 50×80 finite elements in r and z, respectively, and dt is 10 s. Finer discretizations were tested to ensure no detectable loss in accuracy to the number of significant figures presented in the results. For L, $r_1 = 5.1$ cm and $r_2 = 7.4$ cm. For F, the inlet is at (4.5, 50) cm, and the outlets for the enriched and depleted streams are at (7.25, 5) cm and (7.25, 95) cm. The flowrate through each of the two outlets is set as equal, representing a cut of $\theta = 0.5$. A representative liquid at 80 °C and properties of $D = 5 \times 10^{-9}\ m^2s^{-1}$ and $\rho_i = 1000\ kgm^{-3}$ is used. These values are used since they are close to those of several relevant liquids such as water, n-heptane, and carbon tetrachloride (Section S6).

The first considered case is with only countercurrent flow and no inlet/outlet flow. Fig. 2a shows $ln(\alpha)$ vs h for $F = 0$, $L = 20\ ghr^{-1}$, and $v_o = 300$, 400, 500, and 600 ms^{-1}. For example, at $h = 1m$, $ln(\alpha)$ is 0.189, 0.295, and 0.425 for $v_o = 400$, 500, and 600 ms^{-1}, respectively. It can be seen that $ln(\alpha)$ is proportional to both h and ${v_o}^2$. In general, for a fixed L and with $F = 0$, $ln(\alpha)$ is directly proportional to the product of h, ${v_o}^2$, ΔM, and T^{-1}, which aligns with gas analytical models [14]. In real systems, v_o is limited by the strength of the rotor walls and stresses induced within them because of the centrifugation. h is limited by critical speed considerations, equilibrium times, manufacturability, and other engineering considerations. ΔM is determined by the natural stable isotopes of the element(s). T^{-1} is a choice which also strongly impacts the diffusivity and concentration of the fluid and solute.

Fig. 2b shows $ln(\alpha)$ vs L for $F = 0$ and $h = 0.5$ to 1.5 m. For $F = 0$, $ln(\alpha)$ shows a maximum value of $0.297 \times h(m)$ at L = 12 g/hr. This can be understood as in the limit of $L = 0$, there is no countercurrent which contributes to the boosted separation factor of the method. The two outlets have the same r (radial distance) so there is no separation in this limit. Meanwhile, in the limit of $L = \infty$, the fluid inside the centrifuge is being circulated so rapidly that it is mixed everywhere, leading to no separation. Moreover, the maximum $ln(\alpha)$ is achieved when the isotope remixing driven by the back diffusion optimally balances the isotope separation enabled by the countercurrent flows.

A large $ln(\alpha)$ is achievable at $F = 0$, but it diminishes as F increases. For instance, Fig. 2c illustrates the dependence of $ln(\alpha)$ on F for L ranging from 20 to 150 g/hr, showing a consistent decrease in the separation factor across all cases. Therefore, to evaluate the separating

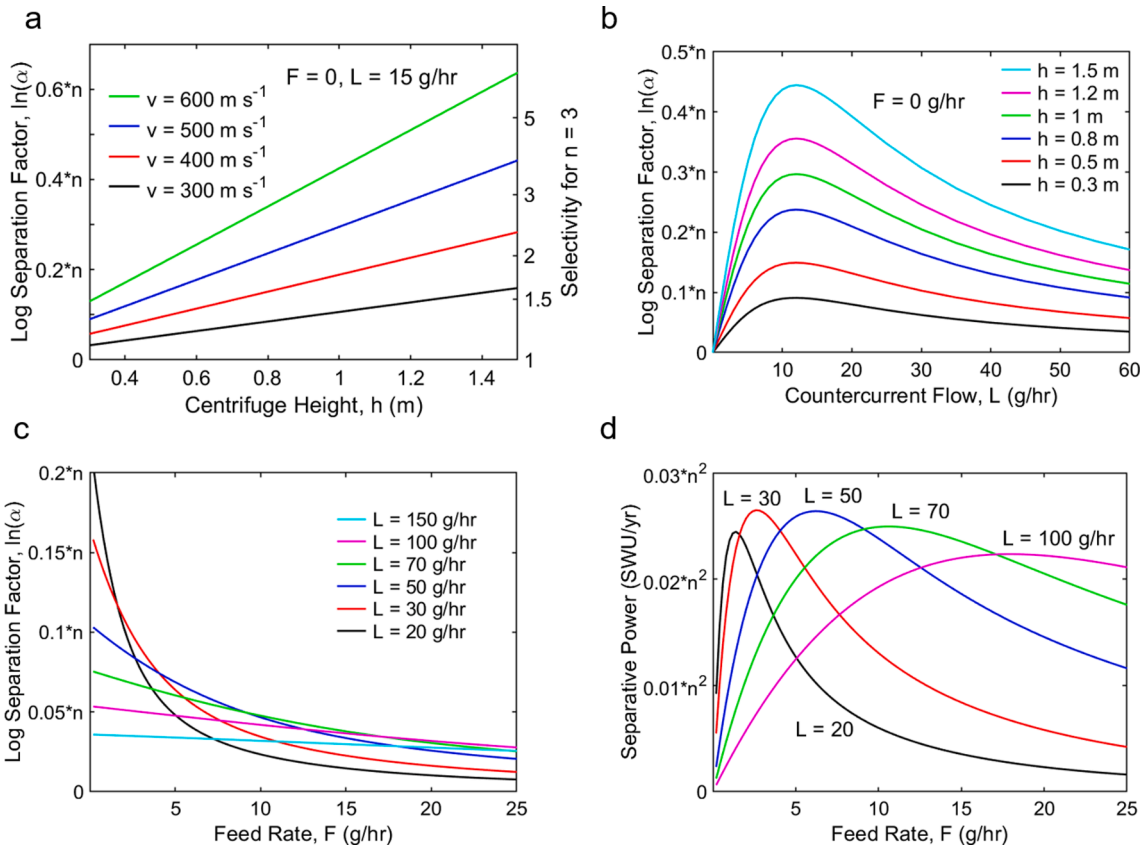

Fig. 2. The performance characteristics for a range of centrifuge conditions simulated. (a) shows the separation factor (per neutrons difference, n) vs. centrifuge height for a range of peripheral velocities. $v_o = 471 ms^{-1}$ and $h = 1m$ is used for all other simulations. (b) shows the separation factor vs. countercurrent flowrate for a range of centrifuge heights. (c) shows the separation factor vs. feed rate for range of countercurrent flowrates. (d) shows the separative power vs. feed rate for range of countercurrent flowrates.

effectiveness of liquid centrifugation, the separative power (δU) is used as shown in Fig. 2d. The separative power, expressed in Separative Work Units (SWU) per year, is defined in Eq. (6). N_i represents the binary isotope ratio, F is the inlet flow in kg/yr, and P and W are the product and waste flows (enriched and depleted), respectively. Eq. (6) can be written as Eq. (7) for a single centrifuge in the case where the two outlet streams are equal in magnitude, with the approximation involving $ln^2(\alpha^*)$ being accurate to within 1 % up to $\alpha = 2$. Therefore, the separative power of a liquid centrifuge is proportion to $v_o^4(\Delta M)^2 T^{-2}$, which is the same product for gas centrifuges. It is worth noting that in high-speed gas centrifuges the proportionality to ${v_o}^4$ cannot be achieved in practice, since the gas is compressed onto the outer wall to such an extent that there is effectively a vacuum at much of the inner portions of the centrifuge [18]. This means that sub-optimal countercurrent flows and fluid collection must be done, resulting in a δU proportional to v_o^2 as shown in Fig. 4c. This limitation does not exist for liquids since they are effectively incompressible, meaning that the proportionality to v_o^4 has no theoretical limit.

$$SWU = P(2N_P - 1)ln\left(\frac{N_P}{1-N_P}\right) + W(2N_W - 1)ln\left(\frac{N_W}{1-N_W}\right) - F(2N_F - 1)ln\left(\frac{N_F}{1-N_F}\right) \quad (6)$$

$$\delta U_{Unit} = F^*\left(2\frac{\sqrt{\alpha^*}}{1+\sqrt{\alpha^*}} - 1\right)ln\left(\sqrt{\alpha^*}\right) \approx \frac{F^* ln^2(\alpha^*)}{8} \quad (7)$$

Varying the height of the centrifuge was also found to impact the separative power. The maximum separative power for $h = 0.5\ m$, $1\ m$, and $1.5\ m$ was $\delta U = 0.0121 \times n^2 SWU/yr$, $0.0268 \times n^2 SWU/yr$, and $0.0416 \times n^2 SWU/yr$, respectively. 'n' represents the number of neutrons separating the isotopes of interest. The corresponding optimal values of F^*, L^*, and $ln(\alpha^*)$, were $F^* = 4.2\ g/hr$, $L^* = 29\ g/hr$. $ln(\alpha^*) = 0.0515 \times n$ for $h = 0.5\ m$, and $F^* = 4.0\ g/hr$, $L^* = 38\ g/hr$, $ln(\alpha^*) = 0.0786 \times n$for $h = 1\ m$, and $F^* = 3.8\ g/hr$, $L^* = 46\ g/hr$. $ln(\alpha^*) = 0.0999 \times n$for $h = 1.5\ m$. All other simulation parameters were identical. Therefore, the separative power grew at a rate slightly faster than linear over the range of heights considered, with F^* staying approximately fixed and $ln(\alpha^*)$ growing slightly faster than $\sqrt{h}$.

3.2. Cascading and process engineering

The trends for the separative power curves for pure liquids shown in Fig. 2, as well as dissolved salts in Fig. S3 of Section S4, exhibit identical qualitative features to countercurrent gas centrifuges [18,20]. This means that F can be varied with predictable and small changes in δU. This is necessary for cascades and high-volume production. It can be noted that a value of $F = 10\ g/hr$ is equivalent to 87.6 kg/yr per machine. Thousands of such machines can be assembled into a cascade to achieve high degrees of enrichment and throughput. Moreover, the results account for many liquids at once, such as water, $TiCl_4$, VCl_4, MoF_6, and Fe $(CO)_5$.

The maximum in separative power for the machine simulated occurs at $F = 4\ g/hr$ and $\alpha = 1.0818^n$. With these parameters, a cascade can be designed to achieve a particular overall enrichment and quantity of desired material. The equations governing ideal cascade dynamics are given by Cohen [14]. A hypothetical modular cascade producing 10 kg/yr of 99.9 % enriched material starting from 5 % can then be quantified.

Fig. 3a and 3b show $ln(\alpha)$ vs F and δU vs F, respectively, for the region around optimal L and F. Understanding the behavior of the centrifuge in

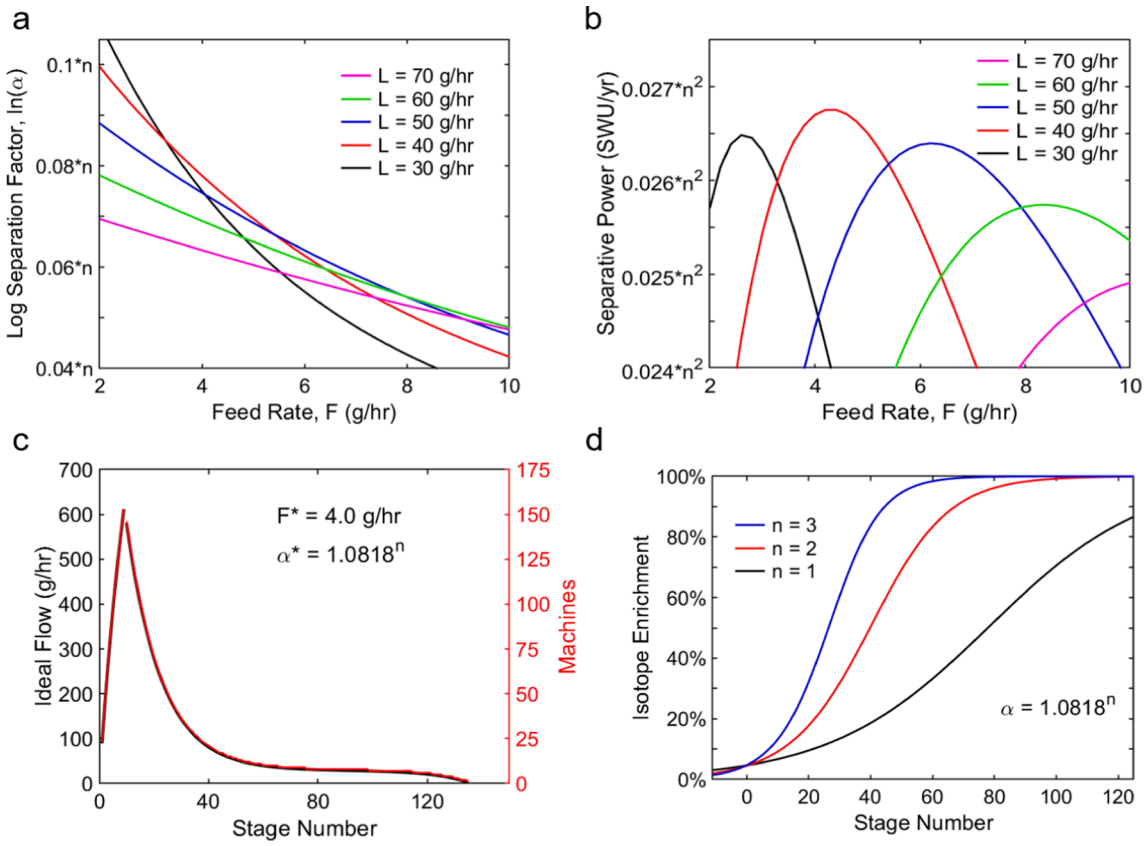

Fig. 3. The performance of the simulated liquid centrifuges in the region of maximum separative power and their subsequent use in a cascade. (a) shows the separation factor vs. feed rate for a range of countercurrent flowrates near the maximum separative power. (b) shows the separative power vs. feed rate for range of countercurrent flowrates in this region. (c) shows the ideal total mass flowrate and number of machines at each stage of the ideal cascade. (d) shows the isotope enrichment vs stage number for range of isotope mass differences.

this region is important to accessing its robustness to various flowrates, countercurrent speeds, and fluids. It also allows for cascade operators to make decisions based on the tradeoffs between product enrichment and quantity after being built. In all cases, the separation factor decreases with increasing feed rate, so there is a direct tradeoff between enrichment and quantity.

Using the specifications of $F^* = 4.0\ g/hr$ and $\alpha^* = 1.0818^n$, a cascade of 138 stages with 3555 total machines satisfies the requirements of a cascade producing 10 kg/yr of 99.9 % enriched material starting from 5 %, assuming a waste depletion to 2.5 % and $\Delta M = 2$ Da to represent a typical element, such as $^{98}Mo/^{100}Mo$, $^{54}Fe/^{56}Fe$, or $^{16}O/^{18}O$. For context, similarly sized or larger gas centrifuges are currently deployed in the many millions to meet the global supply of enriched uranium for the nuclear fuel cycle [21,22]. Fig. 3c shows total mass flow and Machines vs Stage Number for 5 % to 99.9 % enrichment at $\Delta M = 2\ gmol^{-1}$, $N_w = 2.5$ %, and $p = 10\ kg/yr$. (1.14 g/hr). Fig. 3d shows the enrichment percentage vs stage number for the 138-stage cascade for $\Delta M = 1$, 2, and 3 $gmol^{-1}$.

3.3. Performance dependencies

The results above are for a pure liquid and centrifuge with prespecified parameters, but it is important to understand how all results vary as a function of other parameters to generalize the behavior of liquid centrifuges as far as possible, such as diffusivity, density, and temperature as below.

1) Diffusivity (D). High D linearly accelerates all flux terms except for advection. Therefore, L^* and F^* can both be increased in proportion to D, resulting in a linear gain in optimal δU and throughput, with the same separation factor.
2) Partial density (ρ_i) and fluid density (ρ). High ρ_i linearly increases mass throughput. The partial density, ρ_i, is the product of the isotope concentration in mol/m^3 and the isotope molecular mass in kg/mol. High ρ leads to more stress on the centrifuge walls and therefore a reduced speed is likely necessary. Higher fluid density alternatively requires thicker rotor walls, both of which increase the second moment of area and decrease the critical speed.
3) Rotational velocity (ω). Increases α and δU as discussed, but also increase the wall stresses.
4) Centrifuge scale, S, for same v and h/r aspect ratio. Reducing the scale reduces the equilibrium time by S^2, and the volume and mass of the machine by S^3, and reduces the F^* and δU by S. The separation factor is unchanged as long the aspect ratio and peripheral velocities are the same.
5) Temperature (T). Lower temperature increases α, δU, and ρ, but this typically lowers D significantly.
6) Feed material price, \$/kg. Cheaper feed materials mean N_w can be increased resulting in fewer centrifuges needed in the overall cascade for the same N_f.
7) Mass difference, ΔM. Higher increases α and δU. The dependence for δU goes as $(\Delta M)^2$.

Each of these trends and dependencies are precisely the same as for gas centrifuges and can therefore be used as a comparison for the separative power throughput [14,18,20]. Similar simulations to those performed for liquids were also computed for gases in Fig. S4 of Section S5. The same four subfigures presented in Fig. 2a–d were also computed

for a gas in Fig. S4a–d, and the differences between them can be attributed to differences in fluid properties only. For example, the peak of $ln(\alpha)$ with respect to height and countercurrent flowrate for liquid (Fig. 2b) and gas (Fig. S4b) has the same magnitude for a given ΔM and T, while the corresponding value of L for the maximum mainly arises from $D\rho_i$ ($L = 12\ g/hr$ for liquid and $\sim 80\ g/hr$ for gas). This reason also applies to Fig. 2c and Fig. S4c, along with Fig. 2d and Fig. S4d. In all cases, the separation factor is proportional to ΔM and T, while the corresponding values of L and F relate to the magnitude of $D\rho_i$.

Fig. 4a–c show the effects of liquid/gas properties on the separative power, and Fig. 4d shows the effect of scaling the physical size of a centrifuge. As shown in Fig. 4b for H_2O, the $D\rho_i/T^2$ value for liquids is typically within a factor of 2–5 the optimal value of the gaseous phase, with exceptions. The most important exceptions may be the hexafluorides, including MoF_6 for ^{100}Mo and UF_6. Nuclear magnetic resonance (NMR) measurements indicate very fast self-diffusion in liquid MoF_6, WF_6, and UF_6, such that the $D\rho_i$ product can exceed the gas value at temperatures between 60 °C–100 °C, opening the possibility of competing with the gas centrifuge throughput in these cases [23]. In general, the separative throughput of a liquid centrifuge can theoretically be within one order of magnitude of gas centrifuges, while being available to many more elements which do not form stable gas molecules at practical conditions.

4. Discussion

In general, there are striking process engineering similarities to existing gas centrifuges. An interesting similarity to consider is that for all isotope centrifugation δU is proportional is $D\rho_i$, which is a constant at isothermal conditions for a given gas or pure liquid. This means that for the same dimensions of machine a direct comparison of gas/liquid methods can be made. In general, the $D\rho_i$ product for gas phases is 2–5 times higher, which facilities uranium enrichment on the scale of thousands of tons of throughput per year [20,21]. Fortunately, tens of kilograms annually would exceed the global supply for practically all isotopes as of 2024, and this could optimistically increase accessibility to many important nuclear medicine applications.

For elements which have neither a stable gaseous or liquid molecule near ambient conditions, an aqueous salt solution can always be used for isotope centrifugation. For example, Group 1, Group 2, the lanthanides, and numerous transition metals and post-transition metals. In these cases, $D\rho_i$ will vary as a function of salt concentration, and salt concentration gradients will be induced via the centrifugation. The impacts and generalizations of this for achieving high-throughput separation for all elements are discussed further in Section S4. In general, the same principles involving the throughput being proportional to $D\rho_i$ apply.

One key advantage of centrifugation is that it is element independent and its effectiveness depends on ΔM only, which is not the case for chemical exchange, distillation, or most other separation methods. This means that the same machines and cascade can be used for multiple elements or liquids, even simultaneously like H and O in H_2O or Ti and Cl in $TiCl_4$. If multiple isotopes are present, a series of cascades can be used to target each of them, as can be done with gas centrifugation and other mass-dependent methods [14]. For example, such a cascade could be used to meet new market demand from discoveries in real time, instead of lagging behind by many years due to development costs and

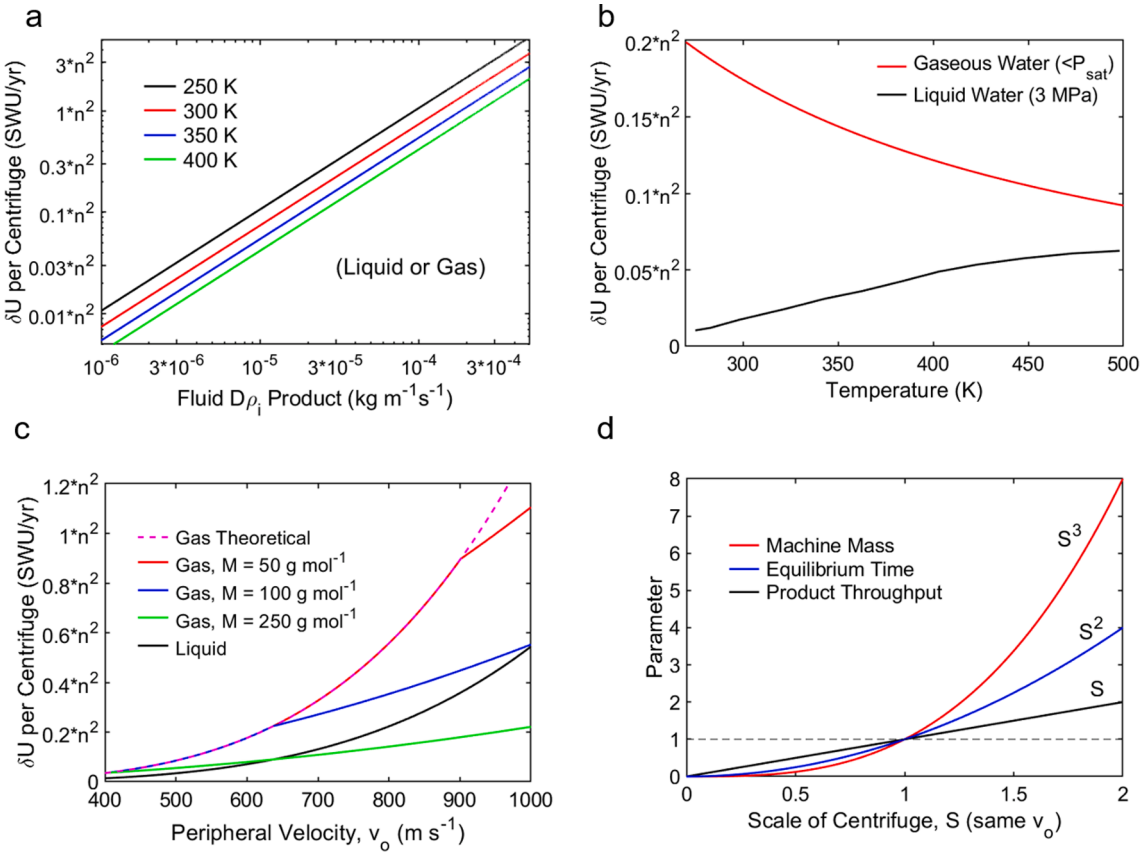

Fig. 4. Generalizations of a centrifuge when used with different fluids. (a) shows the maximum separative power as a function of diffusivity, partial density, and temperature, $D\rho_i/T^2$. These properties can be used to locate optimal operating phases and conditions. (b) shows the separative power versus temperature for gaseous and liquid water due to $D\rho_i/T^2$. (c) shows the separative power versus peripheral velocity for a liquid and gas centrifuge. $D\rho_i$ is assumed 2.5 × greater for the gases, though heavier gaseous molecules are limited at high speeds by the effect of impractically low pressures at smaller radii, reducing δU from v_o^4 to v_o^2 dependence [18]. (d) shows how various centrifuge parameters vary with the physical scale of a centrifuge.

timelines. It is important to note that the ideal cascade configuration is sensitive to both $ln(\alpha)$, i.e. $(\Delta M)^2$, and the natural abundance of the desired isotope (N_f), as outlined in Cohen [14]. Therefore, the centrifuges in an array would need to be reconfigured to best separate a particular isotope, although non-ideal separation still occurs in parallel for elements which are not the primary target of the process.

In general, the technology for gas centrifuges is much more mature, though the liquid case is more general with lower throughput, which should quell any nuclear proliferation concerns about the technology. The ability for a cascade to safely and broadly separate isotopes is shown in Fig. 5 and Table 1.

A small selection of natural isotopes is shown to represent the generality in Fig. 5. The equation of the curve is defined by Eq. (6) by setting $P = 1\ kg$, $N_P = 0.999$ (99.9 %), and $N_W = N_F/2$. F and W are found by ensuring mass conservation of the isotopes. Table 1 shows how these values can be used to calculate the production per year for a given number of centrifuges of the type modelled here. An important consideration is the choice of molecule/solution for a given element. In general, trade-offs exist between throughput, cost, safety, and machine compatibility. For example, in the case of lithium, there are two noteworthy forms, being $LiCl_{(aq)}$, and molten $Li_{(l)}$. While $LiCl_{(aq)}$ is easy to handle and has limited corrosiveness, molten $Li_{(l)}$ has the greatest $D\rho_i$ ($\sim 3.5 \times 10^{-6}\ kgm^{-1}s^{-1}$ vs $\sim 1.5 \times 10^{-7}\ kgm^{-1}s^{-1}$ for 5 M $LiCl_{(aq)}$) [24] but is especially difficult to handle and has a melting point around 180 °C. In general, a safe and non-hazardous aqueous chloride or nitrate solution exists for practically every non-noble-gas element, however, greater throughputs are possible in liquid or gaseous molecules involving fluorine, chlorine, hydrogen, carbonyl, methyl, or ethyl bonds [25].

An important consideration is the pressure–temperature phase diagram of the chosen molecule or solution. The pressure within an incompressible fluid will vary quadratically as a function of radius inside a cylindrical centrifuge, as given in Eq. (8), where $\boldsymbol{P_i}$ is the pressure at the inner radius, r_i. For values of $\boldsymbol{P_i} = 1\ MPa$, $\rho = 1000\ kgm^{-3}$, $\omega r_o = v_o = 471\ ms^{-1}$, and $r_i = r_o/3$, the pressure at the periphery is 67 MPa. Pressures in this range are not typically high enough to significantly impact the melting point, diffusivity, or density of a liquid, which allows for their assumed constancy in the simulations [26]. However, the value of $\boldsymbol{P_i}$ can be used to greatly enhance the boiling point of the fluid, and therefore the temperature of operation and therefore the $D\rho_i$ product. In general, the gain in $D\rho_i$ far outweighs the loss in T^{-2} by operating the centrifuge at a higher temperature in the range of 0 °C to >100 °C. Therefore, the strategy of pressurizing the centrifuge via the inlet and outlet ports to several MPa is likely favorable for increasing overall separative power.

$$\boldsymbol{P} = \boldsymbol{P_i} + \frac{1}{3}\rho\omega^2(r^2 - r_i^2) \tag{8}$$

The purity requirements for the stable precursors of radionuclides used in radiopharmaceuticals can vary based on the specific production process, i.e. cyclotron, linear accelerator, nuclear reactor, or photonuclear reactions, as well as the intended use of the radionuclide [27]. Typically, 90–98 % is sufficient in most cases. In general, higher purity levels of the stable precursor isotopes lead to better yields and higher specific activity of the produced radionuclides, which is particularly important for medical applications since the impurities lead to unwanted radioactive byproducts which may be exposed to patients and medical staff.

The large-scale production of pure isotopes could also lead to numerous unknown benefits due to the abundance of highly enriched isotopes. For example, advanced light-weight and high-strength spaceflight materials or centrifuges made from alloys of ^{46}Ti or ^{54}Fe, ^{6}Li in fueling fusion reactors, ^{192}Os as the densest stable material at ambient conditions, or ^{48}Ca for uncovering new physics. The lanthanides in particular offer many potential radiopharmaceutical applications since they contain 9 elements with multiple isotopes, totaling to 49 natural isotopes which have been inseparable at scale [28]. The lanthanides do not form any molecules which can be easily gasified near ambient conditions, but they can all be highly dissolved in water as a nitrate solution.

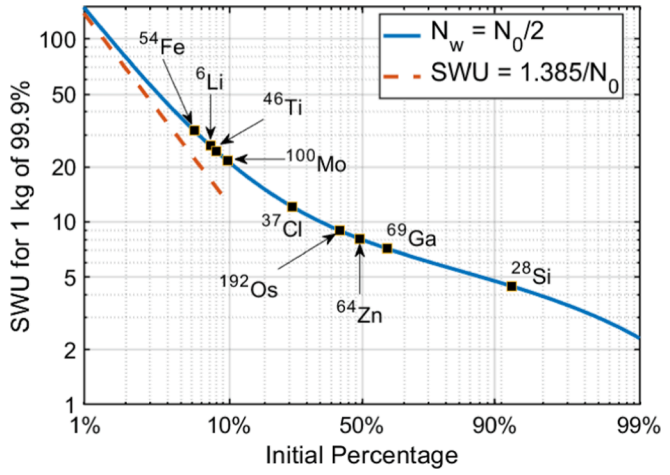

Fig. 5. Shows SWU required vs N_0 for numerous important isotopes to reach 1 kg of 99.9 % purity. The waste stream assay is set at half the natural abundance, so 12 % for ^{37}Cl, which is naturally 24 %.

5. Future work and challenges

Introduced in 2023, the liquid centrifuge method for isotope separation is still in its early stages, primarily demonstrated in batch-based operations that align with modeling results. The main experimental challenge lies in developing continuous-operation machines capable of extensive validation, requiring innovative approaches beyond traditional turbomachinery and gas centrifuge designs, such as avoiding leakage, feed design, and stabilization. Future research should focus on designing affordable, reliable, and high-speed liquid centrifuges, with efforts targeted towards the experimental validation of these systems under continuous operation conditions. This advancement will not only confirm the theoretical predictions presented but also propel the practical application of liquid centrifuge technology in isotope separation.

In adapting technologies from gas to liquid centrifuges, key mechanical innovations can be directly applied. For example, stiff bottom pivot bearings and flexibly mounted neodymium magnetic bearings can be tuned for favorable critical speeds and damping of the rotor, such that stable acceleration to full speed can be achieved while greatly minimizing bearing losses compared to other continuous centrifuge designs [17]. Holweck molecular pumps and a contactless electric motor may also be similarly used to minimize all other sources of power loss. Finally, solutions like in-line variable speed pumps may be used to transport all streams between stages in the cascade, while providing the necessary fluid pressure to feed and withdraw from the centrifuge and induce the countercurrent flow.

With these strategies, we believe that a countercurrent liquid centrifuge can achieve the speeds discussed in this work (e.g., 400–500 ms^{-1}) without leakage. The energy consumption, although likely several times higher than gas centrifuges due to the greater mass, moment of inertia, and viscous drag in the liquid system, will be optimized through these technologies, and is not anticipated to be numerous orders-of-magnitude higher. The mechanical design and prototyping of liquid centrifuges, addressing these specific challenges, will form the basis of future work.

6. Conclusion

Enriched isotopes have propelled significant advancements in

Table 1
Separative power of prototypical centrifuges used for various isotopes.

Isotope	Phase (80 °C)	SWU for 1 kg of 99.9 %	ΔM(g/mol)	$D\rho_i(\times 10^6)$	SWU/yr per 1000 machines	kg/yr per 1000 machines
^{6}Li	5 M $LiCl_{(aq)}$	26.1	1	0.12	0.64	0.025
^{6}Li	$Li_{(l)}$ (200 °C)	26.1	1	3	16	0.62
^{7}Li	$Li_{(l)}$ (200 °C)	4.4	1	3.5	16	4.3
^{18}O	$H_2O_{(l)}$	703	2	6	~170	0.25
^{28}Si	$(C_2H_5)_3SiH_{(l)}$	4.5	1	~0.5	~3	~0.6
^{37}Cl	$CCl_{4(l)}$	12.2	2	3	67.6	5.5
^{46}Ti	$TiCl_{4(l)}$	24.3	1	~1	~6	~0.22
^{48}Ca	5 M $CaCl_{2(aq)}$	752	4	0.72	~61	0.08
^{54}Fe	$Fe(CO)_{5(l)}$	31.2	2	~1.2	~26	~0.8
^{64}Ni	$Ni(CO)_{4(l)}$	159	2	~1.5	~32	~0.2
^{64}Zn	$(C_2H_5)_2Zn_{(l)}$	8.1	2	~2	~43	~5.3
^{69}Ga	$Ga_{(l)}$	7.1	2	10	~210	~30
^{70}Ge	$GeCl_{4(l)}$	13.3	2	~1	~22	~1.6
^{100}Mo	$MoF_{6(l)}$	21.6	2	8	280	8
^{192}Os	$OsF_{6(l)}$	9.0	2	~17	580	~42

various scientific, technological, and medical fields, serving as crucial precursors to vital radionuclides. The development of liquid centrifugation presents a promising method to scale up the production of isotopes, offering flexibility across the periodic table unlike traditional methods. Its operational similarities to gas centrifuges, which are extensively used in nuclear fuel production, may facilitate skill transfer and boost development confidence. Implementing a cascade of countercurrent liquid centrifuges could therefore significantly impact the availability of new materials for diverse applications, contributing to further scientific and technological progress.

Author contributions

J.F.W. conceived the concept. All authors contributed to project planning and data analysis. J.F.W. and Z.H. formulated the model and performed the simulations. All authors wrote the manuscript. Y.Y. and J. F.W. supervised the work.

Funding

This work was supported by Grant No. DE-SC0022256 from the Isotope Program of the United States Department of Energy.

CRediT authorship contribution statement

Joseph F. Wild: Conceptualization, Methodology, Software, Investigation, Writing – original draft, Writing – review & editing, Visualization, Supervision. **Zhinan Han:** Writing – review & editing, Methodology, Formal analysis. **Yuan Yang:** Writing – review & editing, Writing – original draft, Supervision, Project administration, Methodology.

Declaration of competing interest

The authors declare the following financial interests/personal relationships which may be considered as potential competing interests: Provisional patents (U.S. 63/425,181 and 63/548,245) have been filed related to this and prior work.

Data availability

All data are available in the manuscript or the supplementary materials. Information requests should be directed to the corresponding authors.

Appendix A. Supplementary material

Supplementary data to this article can be found online at https://doi.org/10.1016/j.seppur.2024.128046.

References

[1] B. Faubert, A. Tasdogan, S.J. Morrison, T.P. Mathews, R.J. DeBerardinis, Stable isotope tracing to assess tumor metabolism in vivo, Nat. Protoc. 16 (2021) 5123–5145, https://doi.org/10.1038/s41596-021-00605-2.
[2] G. Sgouros, L. Bodei, M.R. McDevitt, J.R. Nedrow, Radiopharmaceutical therapy in cancer: clinical advances and challenges, Nat. Rev. Drug Discov. 19 (2020) 589–608, https://doi.org/10.1038/s41573-020-0073-9.
[3] L. Wang, et al., Spatially resolved isotope tracing reveals tissue metabolic activity, Nat. Methods 19 (2022) 223–230, https://doi.org/10.1038/s41592-021-01378-y.
[4] B.L. Zaret, F.J. Wackers, Nuclear Cardiology, N. Engl. J. Med. 329 (1993), https://doi.org/10.1056/nejm199309163291208.
[5] Meeting Isotope Needs and Capturing Opportunities for the Future: The 201Long Range Plan for the DOE-NP Isotope Progarm, NSAC Isotopes Subcommitee, July 2015 (2015).
[6] R.L. Murray, K.E. Holbert, Nuclear Energy, eighth edition, Chapter 15 - Isotope Separators, Wiley, 2020, pp. 273–289.
[7] L.O. Love, Electromagnetic separation of isotopes at Oak Ridge, Science 182 (1973) 10, https://doi.org/10.1126/science.182.4110.343.
[8] S. Umehara, T. Kishimoto, A. Yanagisawa, CANDLES for double beta decay of 48Ca, J. Phys. 39 (2006), https://doi.org/10.1088/1742-6596/39/1/093.
[9] D.P.M. Fonseca, A.L.M. Feitosa, L.G. Carvalho, R.L. Plaut, A. Padilha, A short review on ultra-high-strength maraging steels and future perspectives, Mater. Res. 24 (2021), https://doi.org/10.1590/1980-5373-MR-2020-0470.
[10] Q. Zhao, Y. Zhao, High-strength titanium alloys for aerospace engineering applications: a review on melting-forging process, Mater. Sci. Eng. 845 (2022), https://doi.org/10.1016/j.msea.2022.143260.
[11] J. Hu, H. Li, Y. Sui, J. Du, Current status and future perspective of radiopharmaceuticals in China, Eur. J. Nucl. Med. Mol. Imaging 49 (2021) 2514–2530, https://doi.org/10.1007/s00259-021-05615-6.
[12] E. Nikolova, D. Tonev, N. Zhelev, V. Neychev, Prospects for radiopharmaceuticals as effective and safe therapeutics in oncology and challenges of tumor resistance to radiotherapy, Dose-Response 19 (2021), https://doi.org/10.1177/1559325821993665.
[13] J.F. Wild, et al., Liquid solution centrifugation for safe, scalable, and efficient isotope separation, Sci. Adv. 9 (2023) eadg8993, https://doi.org/10.1126/sciadv.adg8993.
[14] K.P. Cohen, The Theory of Isotope Separation as Applied to the Large-Scale Production of U-235, McGraw-Hill Book Co., New York, 1951.
[15] A. Boushehri, F.M. Tao, E.A. Mason, Common bulk modulus point for compressed liquids, J. Phys. Chem. 97 (1993) 2711–2714, https://doi.org/10.1021/j100113a037.
[16] M.M. Rahman, W. Liu, M. Lv, H. Pan, Exploring SIMPLE algorithm for all speeds, Ain Shams Eng. J. 14 (2023), https://doi.org/10.1016/j.asej.2022.101854.
[17] S. Whitley, Review of the gas centrifuge until 1962. Part II: principles of high-speed rotation, Rev. Mod. Phys. 56 (1984), https://doi.org/10.1103/RevModPhys.56.67.
[18] E. Ratz, in: H. G. Wood (Ed.), Proceedings of the Fifth Workshop on Gases in Strong Rotation, June 5–9, 1983, University of Virginia, 1983, pp. 55–159.
[19] J.W. Beams, L.B. Snoddy, A.R. Kuhlthau, in: 2nd U.N. Conference on the Peaceful Uses of Atomic Energy, Vol. 4, 1958, pp. 428–434.
[20] A. Glaser, Characteristics of the gas centrifuge for uranium enrichment and their relevance for nuclear weapon proliferation, Sci. Glob. Secur. 16 (2008) 1–25, https://doi.org/10.1080/08929880802335998.
[21] U. S., E. I. A., Uranium Marketing Annual Report (2022).

[22] E. Von Halle, Countercurrent gas centrifuge for the enrichment of U-235, in: Annual AICHE meeting, 1977.
[23] P. Rigny, J. Virlet, Molecular motion and 19F relaxation in the liquid hexafluorides of molybdenum, tungsten, and uranium, J. Chem. Phys. 47 (1967) 4645–4652, https://doi.org/10.1063/1.1701677.
[24] A.L. Ott, Inter-diffusion of li-isotopes in liquid lithium metal, Z. Naturforschg. 20a (1965) 1578–1582, https://doi.org/10.1515/zna-1965-1208.
[25] S.E. Koponen, P.G. Gordon, S.T. Barry, Principles of precursor design for vapour deposition methods, Polyhedron 108 (2016) 59–66, https://doi.org/10.1016/j.poly.2015.08.024.
[26] L. Glasser, Phase diagrams of ordinary water substance, J. Chem. Educ. 81 (2004) 414, https://doi.org/10.1021/ed081p414.
[27] C. Zippel, J. Ermert, K. Kopka, Cyclotrons operated for nuclear medicine and radiopharmacy in the German speaking D-A-CH countries: an update on current status and trends, Nucl. Med. 2 (2022), https://doi.org/10.3389/fnume.2022.850414.
[28] C.S. Cutler, et al., Current and potential therapeutic uses of lanthanide radioisotopes, Cancer Biother. Radiopharm. 15 (2000), https://doi.org/10.1089/cbr.2000.15.531.